Our results support the idea that "silent" histone modifications within large heterochromatic regions are maintained by copying modifications from neighboring preexisting histones (*1*, *24*) without the need for H3-H4 splitting events. However, mechanisms underlying the mitotic inheritance of "active" modifications remain debatable. Our observation that significant amounts of H3.3-H4 tetramers split during replication-dependent nucleosome assembly brings up an intriguing question: Do these tetramer splitting events occur at specific regions of chromatin for specific functions, such as mitotic inheritance (*25*, *26*)? Although we observed significant splitting events only for H3.3–containing tetramers, it remains an open question whether such splitting events are variant-specific or rather chromatin region–specific. We did observe ~2% K8-labeling difference between Flag-H3.1 and copurified H3.1 in several experiments (Fig. 1 and figs. S3 and S4), which could be within our detection error but may also suggest splitting events for a small subset of H3.1–containing tetramers. One possible model is that the replication-dependent nucleosome assembly pathway differs at euchromatic and heterochromatic regions, resulting in specific splitting events, predominantly at euchromatic regions. This is particularly tempting because H3.3 is enriched in euchromatin (*20*, *21*, *27*), and H3.1 histones display a similar modification pattern in the vicinity of H3.3 histones (*22*). Detecting the "splitting hot spots" and unveiling their potential role in the mitotic inheritance of active modifications are interesting directions for future investigation.

References and Notes

1. C. D. Allis, T. Jenuwein, D. Reinberg, *Epigenetics* (Cold Spring Harbor Laboratory Press, New York, 2006).
2. T. Kouzarides, *Cell* **128**, 693 (2007).
3. R. Margueron, P. Trojer, D. Reinberg, *Curr. Opin. Genet. Dev.* **15**, 163 (2005).
4. R. Holliday, J. E. Pugh, *Science* **187**, 226 (1975).
5. T. H. Bestor, *EMBO J.* **11**, 2611 (1992).
6. R. L. Seale, *Cell* **9**, 423 (1976).
7. I. M. Leffak, R. Grainger, H. Weintraub, *Cell* **12**, 837 (1977).
8. G. Russev, R. Hancock, *Nucleic Acids Res.* **9**, 4129 (1981).
9. V. Jackson, R. Chalkley, *Cell* **23**, 121 (1981).
10. V. Jackson, R. Chalkley, *J. Biol. Chem.* **256**, 5095 (1981).
11. A. T. Annunziato, R. K. Schindler, M. G. Riggs, R. L. Seale, *J. Biol. Chem.* **257**, 8507 (1982).
12. C. P. Prior, C. R. Cantor, E. M. Johnson, V. G. Allfrey, *Cell* **20**, 597 (1980).
13. V. Jackson, *Biochemistry* **27**, 2109 (1988).
14. V. Jackson, *Biochemistry* **29**, 719 (1990).
15. K. Yamasu, T. Senshu, *J. Biochem.* **107**, 15 (1990).
16. H. Tagami, D. Ray-Gallet, G. Almouzni, Y. Nakatani, *Cell* **116**, 51 (2004).
17. C. M. English, N. K. Maluf, B. Tripet, M. E. Churchill, J. K. Tyler, *Biochemistry* **44**, 13673 (2005).
18. L. J. Benson *et al.*, *J. Biol. Chem.* **281**, 9287 (2006).
19. R. Natsume *et al.*, *Nature* **446**, 338 (2007).
20. K. Ahmad, S. Henikoff, *Mol. Cell* **9**, 1191 (2002).
21. Y. Mito, J. G. Henikoff, S. Henikoff, *Nat. Genet.* **37**, 1090 (2005).
22. A. Loyola, T. Bonaldi, D. Roche, A. Imhof, G. Almouzni, *Mol. Cell* **24**, 309 (2006).
23. J. J. Pesavento, H. Yang, N. L. Kelleher, C. A. Mizzen, *Mol. Cell. Biol.* **28**, 468 (2008).
24. J. Nakayama, J. C. Rice, B. D. Strahl, C. D. Allis, S. I. Grewal, *Science* **292**, 110 (2001).
25. Y. Nakatani, D. Ray-Gallet, J. P. Quivy, H. Tagami, G. Almouzni, *Cold Spring Harb. Symp. Quant. Biol.* **69**, 273 (2004).
26. A. V. Probst, E. Dunleavy, G. Almouzni, *Nat. Rev. Mol. Cell Biol.* **10**, 192 (2009).
27. S. Henikoff, J. G. Henikoff, A. Sakai, G. B. Loeb, K. Ahmad, *Genome Res.* **19**, 460 (2009).

28. We thank X. Wang from the Howard Hughes Medical Institute/University of Texas Southwestern Medical Center for critical comments on the manuscript. We thank N. Yang and J. Ni for color illustration. We thank P. Mortensen from the University of Southern Denmark for developing and supporting the MSQuant software. This work was supported by the Chinese Ministry of Science and Technology 863 projects 2007AA02Z1A6 (to B. Z.) and 2007AA02Z1A3 (to S.C.).

Supporting Online Material

www.sciencemag.org/cgi/content/full/328/5974/94/DC1
Materials and Methods
Figs. S1 to S9

13 July 2009; accepted 27 January 2010
10.1126/science.1178994

Dynamic Regulation of Archaeal Proteasome Gate Opening As Studied by TROSY NMR

Tomasz L. Religa,[1] Remco Sprangers,[2] Lewis E. Kay[1]*

The proteasome catalyzes the majority of protein degradation in the cell and plays an integral role in cellular homeostasis. Control over proteolysis by the 20*S* core-particle (CP) proteasome is achieved by gated access of substrate; thus, an understanding of the molecular mechanism by which these gates regulate substrate entry is critical. We used methyl–transverse relaxation optimized nuclear magnetic resonance spectroscopy to show that the amino-terminal residues that compose the gates of the α subunits of the *Thermoplasma acidophilum* proteasome are highly dynamic over a broad spectrum of time scales and that gating termini are in conformations that extend either well inside (closed gate) or outside (open gate) of the antechamber. Interconversion between these conformers on a time scale of seconds leads to a dynamic regulation of 20*S* CP proteolysis activity.

The 20*S* core-particle (CP) proteasome is a hollow, barrel-like structure that, through protein degradation, plays an important role in cellular homeostasis (*1*, *2*) and is a target for the design of inhibitors (*3*, *4*). The CP is composed of four homo-heptameric rings. In the case of the archaeal version, discussed here, each ring consists of seven identical monomers ($\alpha_7\beta_7\beta_7\alpha_7$), with the active sites sequestered inside the catalytic chamber formed by $\beta_7\beta_7$ (Fig. 1A) (*5*, *6*). Unfolded substrates enter the CP through the α annulus (Fig. 1, A and B), which is occluded by N termini of the α subunits (the gating residues). Although detailed x-ray structures (*6*–*8*) have established the overall architecture of the isolated archaeal CP, density has not been observed for the gating residues, and the molecular mechanism by which they control entry of substrates remains to be elucidated.

We have previously obtained high-quality ^{1}H-^{15}N transverse relaxation optimized spectroscopy (TROSY) (*9*) and ^{1}H-^{13}C methyl-TROSY (*10*) data sets for α_7 (*11*, *12*), a single-ring version of molecular weight = 180 kilodaltons. The N-terminal 35 residues could not be observed in amide spectra of α_7 (fig. S1), reflecting dynamics on the microsecond-millisecond time scale, which also severely attenuated peaks from isoleucine, leucine, and valine methyl groups in this region (fig. S2). We used a labeling scheme in which highly deuterated $^{13}CH_3$-methionine (Met) proteins were produced (*13*), so that Met methyl groups could be used as probes of structure and dynamics. The 20*S* CP α subunit contains only four natural Met residues, providing spectra of low complexity. To augment the two Met residues (M1 and M6) located in the gating termini, an additional Met residue (M-1) was introduced at the N-terminal end of the protein (Fig. 1C).

Methionine side-chains undergo large-amplitude, fast–time scale motions (*14*) that average out much of the conformational exchange broadening that affects other resonances, allowing high-quality Met methyl-TROSY spectra to be recorded. Figure 1D shows the ^{1}H-^{13}C correlation map of wild-type (WT) α_7. A total of 9 Met correlations were observed in the spectra, subsequently assigned via mutagenesis (fig. S3). Three peaks originate from each M-1 and M1 residue in WT α_7, corresponding to the major state ("A") and a pair of minor states ("B" and "C"). Similar multiple peaks were observed in spectra recorded on the intact WT $\alpha_7\beta_7\beta_7\alpha_7$ CP (Fig. 1D), establishing that they are not an artifact associated with the single-ring structure. Additionally, they do not emerge from the slightly longer-than-normal N terminus (Fig. 1C), as three peaks for M1 are also noted in spectra

[1]Departments of Molecular Genetics, Biochemistry, and Chemistry, University of Toronto, Toronto, Ontario M5S 1A8, Canada. [2]Max Planck Institute for Developmental Biology, Tübingen, Germany.

*To whom correspondence should be addressed. E-mail: kay@pound.med.utoronto.ca

recorded where the α subunit starts at G0 (fig. S4) (*15*). We also noted extra correlations in a construct in which residues Y8 and D9 [which stabilize the open-gate conformation of the proteasome in a complex with the 11*S* activator (*8*)] were mutated to glycine residues (Y8G/D9G α_7). Correlations of states B and C were of higher intensity than in spectra of the wild type, providing more accurate probes of the minor states. Furthermore, in Y8G/D9G α_7, an extra correlation is also observed for M6. Notably, spectra of the monomeric α subunit α_1 contain the "correct" number of peaks (Fig. 1D), indicating that peak duplication is dependent on the formation of ring structures. The fact that similar Met cross peaks are observed in spectra of α_7, $\alpha_7\alpha_7$, and the $\alpha_7\beta_7\beta_7\alpha_7$ 20*S* CP provides strong evidence that the α_7 ring is an excellent model system for the study of proteasome gate structure and dynamics.

We established the identity of these multiple conformations through measurements of paramagnetic relaxation enhancements (PREs) (*16*, *17*), in which nitroxide spin labels are attached to cysteine residues at various positions in the α subunit, and decay rates of either amide or methyl proton magnetization are quantified for the nitroxide label in the oxidized, R_2^{ox}, and reduced, R_2^{red}, states (fig. S5). The PRE effect ($\Gamma_2 = R_2^{ox} - R_2^{red}$) scales as the inverse sixth power of the distance between the unpaired electron of the nitroxide and the nuclear magnetic resonance (NMR) spin, providing a powerful probe of structure. Initially, we quantified amide Γ_2 (Γ_2^{NH}) rates on a sample with a nitroxide attached to position 4 of α_7 (Gly4Cys); Γ_2^{NH} rates were high for residues in helices H1 and H2 (which line the antechamber) with residues on the surface of α_7 being substantially less affected (Fig. 2A). PRE rates of more than 150 s^{-1} for V87 and F91 in H1 indicate a distance between the paramagnetic center and the amide group of less than 17 Å, not consistent with crystal structures (*7*) or a recent cryo–electron microscopy model (*18*). In the latter, the N termini extend outward on the surface of the alpha ring. We were not able to satisfy many of the Γ_2^{NH} rates in structure calculations unless the N terminus of at least one of the seven α subunits in α_7 was allowed to cross the α annulus (Fig. 1B) and extend into the interior of the ring, corresponding to the antechamber in the intact proteasome (Fig. 1B). In this case, all rates could be satisfied. Because Γ_2^{NH} values for residues around positions 80 to 100 were most affected, a spin label was added at position 95 [located >24 Å from the α annulus on the inside of the antechamber (Fig. 1B)], and the effects on the Met correlations quantified by recording methyl-TROSY spectra of both WT (fig. S6) and Y8G/D9G (Fig. 2B) α_7. In the oxidized paramagnetic state, peaks corresponding to sites B and C were completely eliminated, whereas those from the major state (A) showed little change in intensity, with methyl ^{1}H Γ_2 ($\Gamma_2^{CH_3}$) rates of only 3 to 7 s^{-1}. This observation provides strong evidence that states B and C derive from gating residues inside the chamber (the "in" position). Placement of a spin-label at position 20, located above the α annulus and well outside the lumen of the proteasome (Fig. 1B), eliminated peaks from state A (Fig. 2B), establishing that this conformation corresponds to the "out" position for the terminal residues. Once signals from the in and out conformations were assigned, the relative populations of each were quantified from heteronuclear multiple-quantum coherence (HMQC) spectra, as summarized in Fig. 2C. For WT α_7, approximately two termini are inserted into the cavity, on average, very similar to what is quantified for the full 20*S* WT CP. In the case of Y8G/D9G α_7, approximately three termini populate the in state (fig. S7).

We inserted additional spin labels at positions 72, 107, 115, and 143 [located inside the chamber (Fig. 1B, red)], confirming the large differences in ^{1}H $\Gamma_2^{CH_3}$ rates between state A and either of states B and C noted for spin label at position 95 and providing additional distance restraints from which structures of the out and in states could be calculated. The in conformations corresponding to states B and C were not distinguished in structure calculations because a maximum dif-

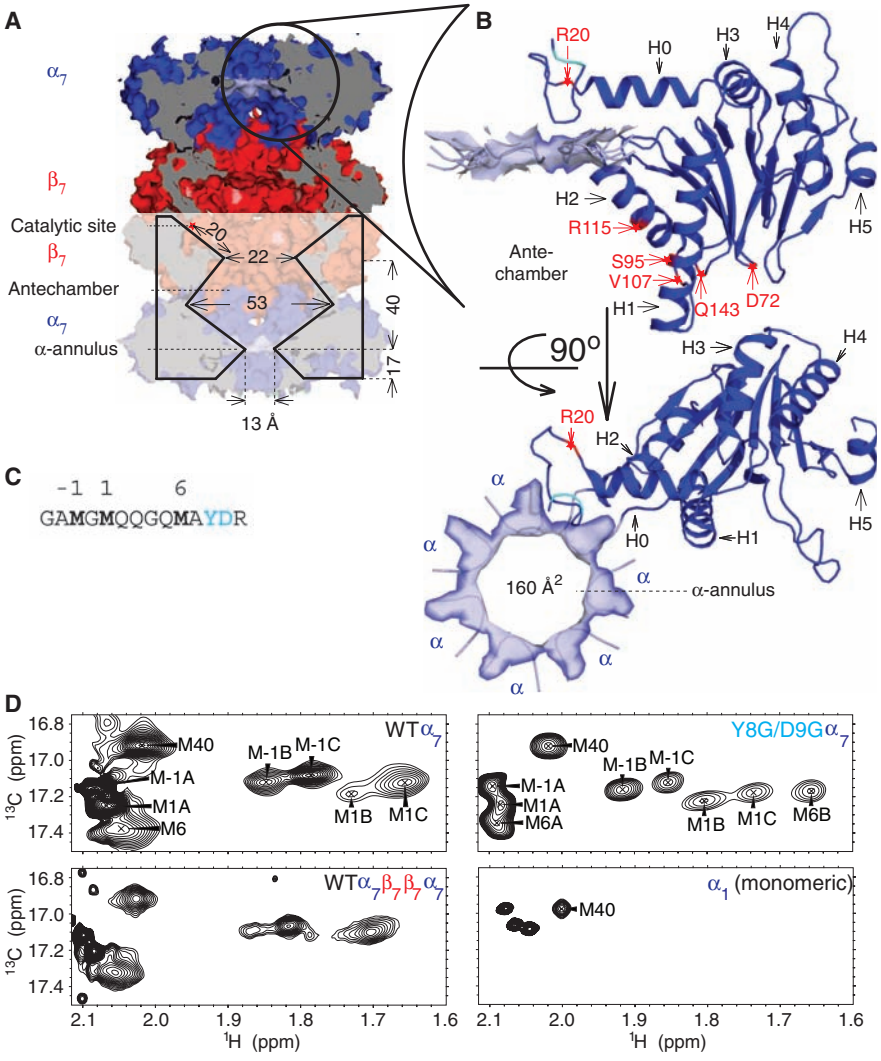

Fig. 1. Multiple conformations for the proteasome gating residues. (**A**) Space-filling, cross-sectional side-view representation of the 20*S* CP proteasome ($\alpha_7\beta_7\beta_7\alpha_7$) from *Thermoplasma acidophilum*, showing the relative positions of the α annulus, the antechambers, and the catalytic chamber, as well as the dimensions of the molecule [PDB accession code 1YA7 (*7*)]. (**B**) Each α ring is composed of seven identical α subunits. A single α subunit is shown in ribbon diagram (two orientations), along with the α annulus that is composed of residues from all seven subunits. The locations of added spin-labels for PRE measurements are indicated in red. (**C**) Primary sequence of the N-terminal α-subunit residues, including GAMG introduced by cloning. The Met residues that we used as probes in this study are shown in bold. When YD residues (in light blue) are mutated to G residues, the out conformation of the gating residues is destabilized. (**D**) ^{1}H-^{13}C Met methyl HMQC spectra of the WT α_7 ring, WT $\alpha_7\beta_7\beta_7\alpha_7$, and the Y8G/D9G α_7 ring showing multiple correlations for M1, M-1 (denoted by A, B, and C), and M6 (Y8G/D9G α_7 ring, denoted by A and B). Multiple correlations are not observed for the isolated α subunit (bottom). In all spectra, the M120 correlation is outside the spectral window shown here. ppm, parts per million.

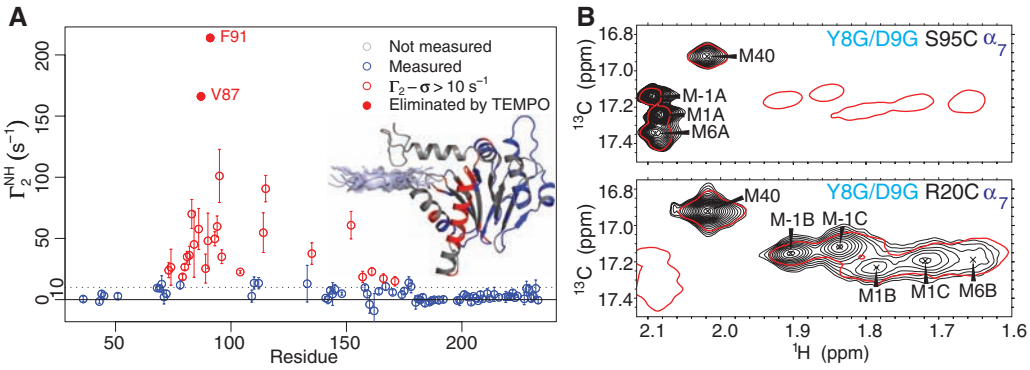

C

Position	OUT	IN
α_7 M-1	A	B+C
WT	76	24
Y8G/D9G	55	45
E25G	87	13
E25P	100	0
	+ 11S	
WT	91	9
Y8G/D9G	56	44

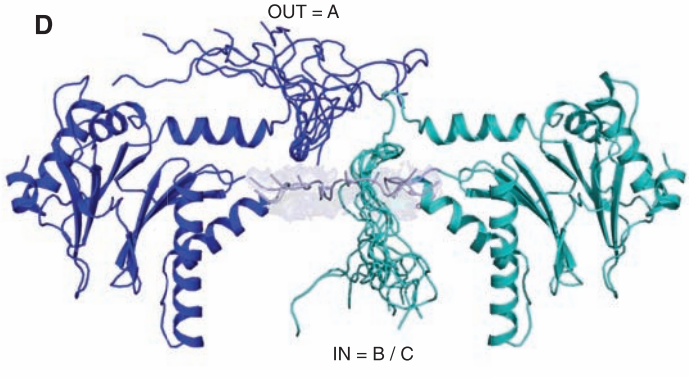

Fig. 2. Assignment of correlations to in and out conformations and calculation of structural ensembles. (**A**) H^N Γ_2 rates quantified on a sample with a nitroxide attached to position 4 of each α subunit. Red open circles indicate those residues for which rates exceed measurement errors (σ) by at least 10 s^{-1}, whereas peaks for V87 and F91 disappeared in the oxidized state (solid red circles). Rates were high for residues in helices H1 and H2 (indicated in red). Note that amides of residues 1 to 35 are not visible in the spectra due to a microsecond-millisecond exchange process (fig. S1) and are thus not available as probes. TEMPO, 2,2,6,6-tetramethyl-1-piperidinyloxyl. (**B**) Superposition of ^{1}H-^{13}C Met methyl HMQC spectra recorded from the Y8G/D9G α_7 ring. Attachment of a spin-label at position 95 (see Fig. 1B) eliminates correlations from states B and C for M1, –1, and 6 (top), whereas a nitroxide positioned at residue 20 eliminates peaks from the A conformation (bottom) (see fig. S6). Spectra recorded with nitroxide in the oxidized (black) and reduced states (red, 1 contour) are shown. (**C**) Relative populations of the out (state A) and in (states B and C) conformations obtained from peak volumes in ^{1}H-^{13}C HMQC spectra. Errors of no more than 2% are estimated based on quantification from multiple spectra. (**D**) Ensembles of 10 structures calculated for WT α_7 showing gating residues in the in (teal) and out (blue) conformations for an α subunit. In WT α_7, approximately two of the seven subunits are in the in state.

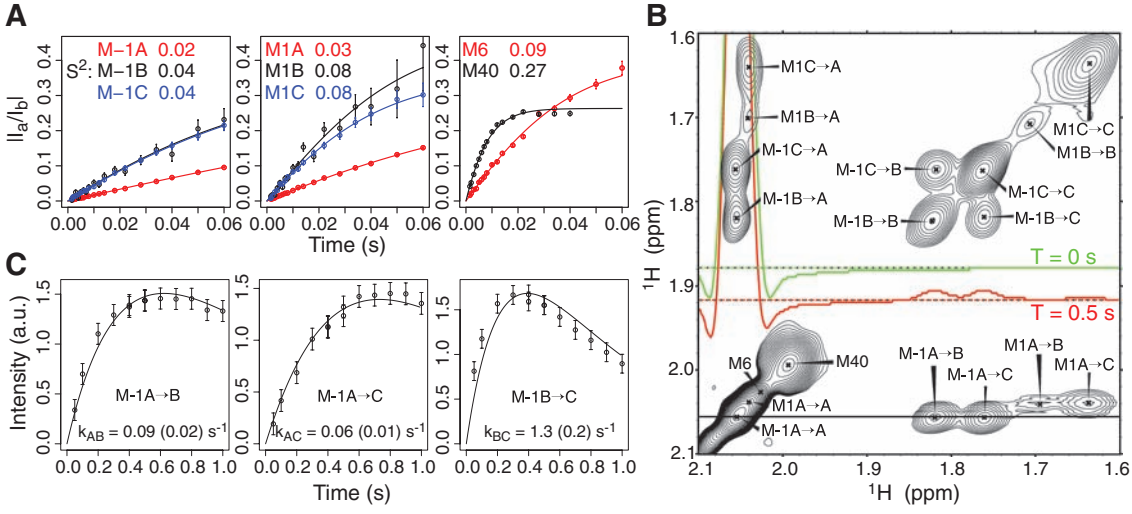

Fig. 3. Proteasome gates are dynamic over a broad spectrum of time scales. (**A**) Ratio of intensities of cross peaks in ^{1}H-^{13}C spectra that are sensitive to the difference (I_a) and sum (I_b) of methyl ^{1}H transitions (*21*); this ratio can be fit (solid lines) to extract methyl axis order parameters (S^2), as listed. (**B**) Magnetization exchange spectroscopy (*22*) showing that states A, B, and C [corresponding to out (A) and in (B and C) gate conformations] are in dynamic equilibrium. Exchange cross peaks are not observed when the exchange mixing time is set to 0 (green trace), but they are present for nonzero values (red). (**C**) The build-up of exchange peaks can be used to quantify exchange rates (k_{mn}).

ference of only 3 Å was noted in a comparison of all spin-label/Met methyl distances involving these states (for the most part, within the error bounds of our measurements). Figure 2D shows the 10 lowest-energy structures corresponding to out and in conformations of a given α monomer within the context of a WT α_7 ring, calculated from a restrained molecular dynamics procedure (*19*) and outlined in the supporting online material (SOM) (*20*). Interestingly, the reverse-turn loop (formed by the conserved residues Y8, D9, P17, and Y26) that stabilizes the open conformation of the proteasome-11*S* activator complex (*8*) is present in most structures of the out state but is always broken in the in state. The in/out configurations deviate considerably around A11, where the backbone starts pointing toward the α annulus for the in state. Termini in the in state

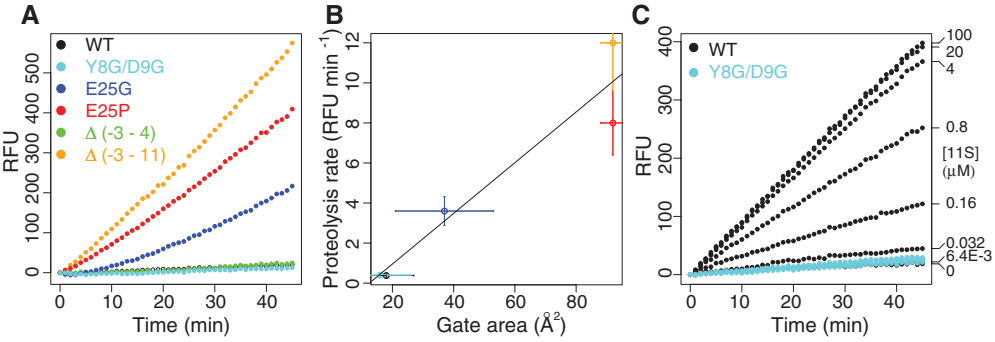

Fig. 4. Proteasome activity correlates with accessible surface area of the α annulus. (**A**) Relative fluorescence units (RFU) versus hydrolysis time of the nine-residue (*31*) Mca-RPPGFSAFK(Dnp)-OH peptide using different 20*S* CP constructs (see SOM), with hydrolysis rates increasing with accessible surface area of the α annulus. (**B**) Correlation of proteasome hydrolysis rates with α annulus–accessible surface area (horizontal error bars are derived from the ensemble of calculated structures, as described in the SOM), color-coded as in (A). (**C**) Binding of the 11*S* activator increases hydrolysis of the nine-residue peptide for the WT (black), but not the Y8G/D9G (light blue), proteasome. Concentrations of 11*S* (per monomer) for each WT CP trace are shown along the right vertical axis. The same range of concentrations was employed for Y8G/D9G, with little effect. The proteasome concentration (in monomer) was 2 nM (A) and 4 nM [(C), 11S binding]. The curves in (A) and (C) are representative from at least 4 separate measurements, with errors in estimated rates (slope of the curves) up to 20%.

cross the annulus at residues A7 to R10 (depending on the structure), effectively closing the α annulus to substrate entry. Structures were also obtained for Y8G/D9G α_7 and are very similar to those for the wild type. Notably, each of the ensembles in Fig. 2D shows a major amount of disorder, reflecting to some extent the small numbers of restraints used in structure calculations (table S1). However, the structures also represent what most certainly is a very dynamic gating terminus. For example, measured order parameters squared (S^2) that quantify the amplitudes of methyl-axis picosecond time-scale motion (*21*) are <0.1 for M-1, M1, and M6 (in all states), indicating near isotropic motion characteristic of a high level of dynamics (Fig. 3A).

As a test of our model, we prepared a complex consisting of spin-labeled 11*S* activator with label at position 108 and Met-labeled Y8G/D9G α_7. Because the paramagnet is placed in the lumen of 11*S* at a position accessible only to the out states of the gating residues, it would be expected to substantially attenuate the A-state correlations, whereas those from the B and C states are hardly affected. ^{1}H-^{13}C methyl-TROSY spectra establish that this is indeed the case with A-state peaks eliminated and $^1\mathrm{H}\,\Gamma_2^{\mathrm{CH_3}}$ rates of only $6 \pm 3\ \mathrm{s}^{-1}$ for the minor states (fig. S8). This result provides a strong cross-validation of our proposed model of gating in which α-subunit terminal residues can assume two very distinct states, corresponding to out and in conformations, with activation occurring by shifting the relative populations of each state, leading to an increase in the out conformation.

The in and out states of the gating termini interconvert on the seconds time scale that can be quantified by magnetization exchange spectroscopy (Fig. 3, B and C) (*22*). Figure 3C shows the build-up of peak intensities corresponding to the transfer of magnetization between states j and k ($j \neq k$) during a prescribed time interval that can be fit to extract lifetimes of each state; values on the order of 6.5 s $(k_{AB} + k_{AC})^{-1}$ and 2 s $\frac{1}{2}(k_{BA}^{-1} + k_{CA}^{-1})$ are obtained for the out and in states, respectively, at 45°C (k_{ij} is the rate of interconversion from state i to state j). Whereas, on average, approximately two gating termini lie within the antechamber of the WT proteasome, the experiments reported here indicate a stochastic exchange process that controls the number of in and out termini in any given molecule as a function of time, thereby regulating function.

To establish a correlation between proteasome function and relative population of in versus out gating termini, we performed proteolysis assays on the series of 20*S* CP ($\alpha_7\beta_7\beta_7\alpha_7$) mutants listed in Fig. 4A. Large enhancements of proteolysis rates were observed for the gateless Δ(–3 – 11) mutant (yellow) and for E25P α_7 (red) [only the out states are populated in E25P α_7; no minor states exist in HMQC spectra (Fig. 2C and fig. S9)], clearly indicating that the all-out state corresponds to the completely open form of the gate. As expected, proteolysis was much slower for the E25G mutant, where, on average, slightly less than one of the seven N termini resides in the chamber (Fig. 2C). Slower proteolysis rates were observed for the wild type and the deletion mutant Δ(–3 – 4). As expected, similar rates were quantified because, in both cases, the same number of termini are inside the chamber (approximately two), with the same residues (A7 to R10, see above) blocking the α annulus. We did not observe a major difference in proteolysis rates between WT and Y8G/D9G 20*S* CP, although the population of in termini is considerably higher in the mutant (Fig. 2C). However, a comparison of the accessible surface areas of the α annulus calculated on the basis of the PRE-derived structures shows little difference whether two (WT) or three (Y8G/D9G) termini cross the annulus (18 ± 9 versus 16 ± 10 Å^2), because the bulky residues tyrosine and aspartic acid in the WT have been substituted by glycine in the mutant. Notably, we observed a strong correlation between hydrolysis rates and accessible surface area of the α annulus for the mutants considered in our study (Fig. 4B). Binding of the 11*S* activator to WT 20*S* CP that is known to stabilize the open-gate conformation (*23*) leads to an increase in hydrolysis rates with added activator, whereas no effect is observed for the Y8G/D9G mutant (Fig. 4C). These findings are consistent with the shift in out versus in populations in the case of the wild type [but not for the mutant (Fig. 2C)] and are in agreement with results showing that 11*S* binding to the Y8G/D9G 20*S* CP (fig. S10) cannot open the gate because key interactions are eliminated due to the mutations (*7*, *8*). Finally, very similar results to those for 11*S* binding have been obtained for an 11*S* chimeric construct in which the final 10 C-terminal 11*S* residues are substituted for those from the hexameric proteasome-activating nucleotidase (PAN) (fig. S11) (*24*, *25*). It is worth noting that Archaea contain a hexameric PAN-like activator with the conserved C-terminal hydrophobic-tyrosine-X motif that has been shown to be essential for proteasome binding (*26*).

Thus, gating of the 20*S* CP archaeal proteasome is controlled through highly dynamic N termini that interconvert between conformations that place them either outside or well inside the antechamber, with rates of proteolysis that depend on the relative populations of termini in the in and out states. 20*S* CPs from Archaea and beyond can cleave a variety of different intrinsically disordered proteins (*27*, *28*) in the absence of auxiliary components, and there is growing consensus of the importance of this non-ubiquitin–based degradation pathway (*29*). Additionally, regulation of protein cleavage by the gating termini of the naked 20*S* CP is critical for cell viability (*30*). An understanding of the dynamic mechanism of 20*S* CP gating is therefore important and may open the possibility of regulating proteasome function through the design of drugs that alter the ratio of in versus out conformers or that perhaps change the dynamics of exchange between them.

References and Notes

1. W. Baumeister, J. Walz, F. Zühl, E. Seemüller, *Cell* **92**, 367 (1998).
2. A. L. Goldberg, *Nature* **426**, 895 (2003).
3. A. L. Goldberg, *Biochem. Soc. Trans.* **35**, 12 (2007).
4. G. Nalepa, M. Rolfe, J. W. Harper, *Nat. Rev. Drug Discov.* **5**, 596 (2006).
5. Y. Cheng, *Curr. Opin. Struct. Biol.* **19**, 203 (2009).
6. J. Löwe *et al.*, *Science* **268**, 533 (1995).
7. A. Förster, E. I. Masters, F. G. Whitby, H. Robinson, C. P. Hill, *Mol. Cell* **18**, 589 (2005).

8. A. Förster, F. G. Whitby, C. P. Hill, *EMBO J.* **22**, 4356 (2003).
9. K. Pervushin, R. Riek, G. Wider, K. Wüthrich, *Proc. Natl. Acad. Sci. U.S.A.* **94**, 12366 (1997).
10. V. Tugarinov, L. E. Kay, *J. Am. Chem. Soc.* **125**, 13868 (2003).
11. R. Sprangers, L. E. Kay, *Nature* **445**, 618 (2007).
12. R. Sprangers *et al*., *Biochemistry* **47**, 6727 (2008).
13. I. Gelis *et al*., *Cell* **131**, 756 (2007).
14. A. Mittermaier, L. E. Kay, J. D. Forman-Kay, *J. Biomol. NMR* **13**, 181 (1999).
15. Single-letter abbreviations for the amino acid residues are as follows: A, Ala; C, Cys; D, Asp; E, Glu; F, Phe; G, Gly; H, His; I, Ile; K, Lys; L, Leu; M, Met; N, Asn; P, Pro; Q, Gln; R, Arg; S, Ser; T, Thr; V, Val; W, Trp; and Y, Tyr.
16. J. L. Battiste, G. Wagner, *Biochemistry* **39**, 5355 (2000).
17. G. M. Clore, *Mol. Biosyst.* **4**, 1058 (2008).
18. J. Rabl *et al*., *Mol. Cell* **30**, 360 (2008).
19. C. D. Schwieters, J. J. Kuszewski, N. Tjandra, G. M. Clore, *J. Magn. Reson.* **160**, 65 (2003).
20. Materials and methods are available as supporting material on *Science* Online.
21. V. Tugarinov, R. Sprangers, L. E. Kay, *J. Am. Chem. Soc.* **129**, 1743 (2007).
22. N. A. Farrow, O. Zhang, J. D. Forman-Kay, L. E. Kay, *J. Biomol. NMR* **4**, 727 (1994).
23. F. G. Whitby *et al*., *Nature* **408**, 115 (2000).
24. B. M. Stadtmueller *et al*., *J. Biol. Chem.* **285**, 13 (2010).
25. Y. Yu *et al*., *EMBO J.* **29**, 692 (2010).
26. A. Ruepp, B. Rockel, I. Gutsche, W. Baumeister, A. N. Lupas, *J. Struct. Biol.* **135**, 126 (2001).
27. A. F. Kisselev, T. N. Akopian, A. L. Goldberg, *J. Biol. Chem.* **273**, 1982 (1998).
28. C.-W. Liu, M. J. Corboy, G. N. DeMartino, P. J. Thomas, *Science* **299**, 408 (2003); published online 12 December 2002 (10.1126/science.1079293).
29. P. Tsvetkov, N. Reuven, C. Prives, Y. Shaul, *J. Biol. Chem.* **284**, 26234 (2009).
30. M. Bajorek, D. Finley, M. H. Glickman, *Curr. Biol.* **13**, 1140 (2003).
31. D. M. Smith *et al*., *Mol. Cell* **27**, 731 (2007).

32. We thank J. Forman-Kay for providing laboratory space and for valuable discussions, R. Muhandiram for NMR support, X. Li and A. Shimmer for assistance with the plate reader, and F. Hansen and D. Korzhnev for discussions. T.L.R. acknowledges the European Molecular Biology Organization (ALTF 827-2006) and the Canadian Institutes of Health Research (CIHR) for postdoctoral fellowships. L.E.K. holds a Canada Research Chair in Biochemistry. This work was supported by a grant from the CIHR. The structural ensembles of WT α_7 and Y8G/D9G α_7 have been deposited in the Protein Data Bank (PDB) with accession codes 2ku1 and 2ku2, respectively.

Supporting Online Material

www.sciencemag.org/cgi/content/full/328/5974/98/DC1
Materials and Methods
Figs. S1 to S11
Table S1
References

23 November 2009; accepted 2 March 2010
10.1126/science.1184991

Evasion of CD8$^+$ T Cells Is Critical for Superinfection by Cytomegalovirus

Scott G. Hansen,[1]* Colin J. Powers,[1]*† Rebecca Richards,[1] Abigail B. Ventura,[1] Julia C. Ford,[1] Don Siess,[2] Michael K. Axthelm,[1,2] Jay A. Nelson,[1,2] Michael A. Jarvis,[1] Louis J. Picker,[1,2]‡ Klaus Früh[1,2]‡

Cytomegalovirus (CMV) can superinfect persistently infected hosts despite CMV-specific humoral and cellular immunity; however, how it does so remains undefined. We have demonstrated that superinfection of rhesus CMV–infected rhesus macaques (RM) requires evasion of CD8$^+$ T cell immunity by virally encoded inhibitors of major histocompatibility complex class I (MHC-I) antigen presentation, particularly the homologs of human CMV US2, 3, 6, and 11. In contrast, MHC-I interference was dispensable for primary infection of RM, or for the establishment of a persistent secondary infection in CMV-infected RM transiently depleted of CD8$^+$ lymphocytes. These findings demonstrate that US2-11 glycoproteins promote evasion of CD8$^+$ T cells in vivo, thus supporting viral replication and dissemination during superinfection, a process that complicates the development of preventive CMV vaccines but that can be exploited for CMV-based vector development.

A general characteristic of the adaptive immune response to viruses is its ability to prevent or rapidly extinguish secondary infections by identical or closely related viruses. A notable exception is the herpesvirus family member cytomegalovirus (CMV), which can repeatedly establish persistent infection in immunocompetent hosts (*1*–*3*). Sequential infections are likely the reason for the presence of multiple human CMV (HCMV) genotypes in the human host (*4*). This ability to establish secondary persistent infections despite the preexistence of persistent virus (referred to as "superinfection") is particularly notable because healthy CMV-infected individuals develop high-titer neutralizing antibody responses and manifest very-high-frequency CD4$^+$ and CD8$^+$ CMV-specific T cell responses (>10% of circulating memory T cells can be CMV-specific) (*5*). This evasion of pre-existing immunity has frustrated attempts to develop preventive CMV vaccines (*6*, *7*) but can be exploited for the development of CMV vectors capable of repeatedly initiating de novo T cell responses to heterologous pathogens in CMV-positive hosts (*3*).

The biologic importance of this superinfection capability has prompted our investigation of its extent and mechanism. We previously showed that inoculation of RhCMV$^+$ rhesus macaques (RM) with 10^7 plaque-forming units (PFU) of genetically modified RhCMV (strain 68-1) expressing simian immunodeficiency virus (SIV) antigens resulted in superinfection manifested by the persistent shedding of the genetically modified CMV in the urine and saliva and by the induction and long-term maintenance of de novo CD4$^+$ and CD8$^+$ T cell responses specific for the SIV insert (*3*). To determine whether RhCMV would be able to overcome immunity at lower, more physiologic doses of infection, as reported for HCMV (*7*), a recombinant RhCMV containing a loxP-flanked expression cassette for SIVgag [RhCMV(gagL)] (fig. S1) was inoculated subcutaneously at doses of 10^4 or 10^2 PFU into four RM naturally infected by RhCMV, as manifested by the presence of robust RhCMV-specific T cell responses (table S1A). The SIVgag-specific T cell responses in peripheral blood mononuclear cells (PBMC) or in broncho-alveolar lavage lymphocytes (BAL) were monitored by flow cytometric analysis of intracellular cytokine staining (ICCS) (figs. S2 and S3) after stimulation with consecutive overlapping 15–amino acid peptides corresponding to SIVgag (*8*). Reduction of the inoculating dose had minimal impact on superinfection dynamics: All animals developed SIVgag-specific T cell responses within 2 weeks (Fig. 1A), and secretion of SIVgag-expressing virus in urine or buccal swabs was observed within 4 to 10 weeks of infection in both cohorts (Fig. 1B). The time to first detection of secreted virus in these low-dose-challenged RM was not materially different from that of eight RhCMV$^+$ animals infected with 10^7 PFU of RhCMV(gagL) (Fig. 1B). Moreover, the SIVgag-specific T cell responses and RhCMV(gagL) secretion were stable for more than 3 years regardless of initial dose (Fig. 1, A and C). These data indicate that, consistent with HCMV in humans, RhCMV is able to overcome high levels of CMV-specific immunity and to establish secondary persistent infections, even with low doses of challenge virus.

We hypothesized that an essential step during CMV superinfection is the ability of the virus to clear an initial immunological checkpoint. A likely candidate for such an immunological barrier is CD8$^+$ cytotoxic T cells (CTL), because they are crucial for controlling CMV-associated diseases (*9*). The importance of CTL control for CMV is also suggested by viral expression of multiple proteins that inhibit presentation of viral peptide antigens to CD8$^+$ T cells via major histocompatibility complex class I (MHC-I) molecules (*10*). HCMV encodes at least four related glycoproteins, each with a unique mechanism to

[1]Vaccine and Gene Therapy Institute, Oregon Health and Science University, 505 Northwest 185th Avenue, Beaverton, OR 97006, USA. [2]Oregon National Primate Research Center, Oregon Health and Science University, 505 Northwest 185th Avenue, Beaverton, OR 97006, USA.

*These authors contributed equally to this work.
†Present address: Salk Institute for Biological Studies, 10010 North Torrey Pines Road, La Jolla, CA 92037, USA.
‡To whom correspondence should be addressed. E-mail: pickerl@ohsu.edu (L.J.P.); fruehk@ohsu.edu (K.F.)

Dynamic Regulation of Archaeal Proteasome Gate Opening As Studied by TROSY NMR

Tomasz L. Religa, Remco Sprangers, and Lewis E. Kay

Science, 328 (5974), • DOI: 10.1126/science.1184991

Open Sesame

The proteosome plays a key role in cellular homeostasis through catalyzing protein degradation. It is a barrel-shaped nanomachine whose activity is regulated through gating substrate entry. Religa *et al.* (p. 98) now show that N-terminal gating residues in the proteasome interconvert on a second's time-scale between conformations that place them either outside or inside the proteasomal antechamber. An increase in the number of termini occupying the “in” state decreased rates of hydrolysis. Furthermore, proteasome activators known to increase the proteolysis rate lead to an increase in the number of termini in the “out” state.